Levitated magnetic particles as ac magnetic field sensors

A. T. M. Anishur Rahman*

Electromagnetic waves are widely used in sophisticated defense applications, biomedicine and fundamental science. Their efficient detection determines how we communicate, defend against adversaries, diagnose diseases and perform search and rescue operations. In this article, exploiting the precession of a levitated magnetic particle in ultra-high vacuum, it is shown that weak electromagnetic waves down to femtotesla level can be detected. It is also shown that such a sensor has a large dynamic range over a millitesla, is continuously tunable over many gigahertz and can detect frequencies with a sub-hertz resolution. It is argued that the new magnetometer can be used as a receiver for electromagnetic waves in areas such biomedicine, search and rescue, and defense.

The ability to detect weak electromagnetic (EM) fields has applications in fundamental science [1–3], radar [4], biomedicine [5, 6], search and rescue [7] and consumer electronics [8]. Traditionally, such signals are detected using antennas which once made cannot be changed and have a limited frequency range of operations. In principle, EM fields can be detected using either an electric or a magnetic field sensor. Examples of electric field sensors include Rydberg atoms [9, 10]. Such a sensor has a large frequency range of operation e.g., from MHz to THz [9, 11]. Their sensitivities in the free space configuration can be on the order of a μV/m (3×10^{-14} T) [9, 10, 12]. Such electric field detectors detect discrete frequencies and require tunable lasers. Existing magnetic field sensors such as atomic vapours [13] and the nitrogen-vacancy centre (NVC) in diamond based sensors [14] are predominantly used as dc field sensors, although some progress has been made towards the detection of EM fields using NVCs in diamond [15]. Such magnetic field sensors have a relatively small dynamic range e.g., $\leq \mu T$. Atomic vapour-based sensors also require magnetic shields. Superconducting quantum interference devices-based magnetometers are excellent magnetic field sensors but require cryogenic temperatures [16].

Levitation in vacuum provides a contactless and a near-frictionless environment. This makes levitated particles very susceptible to external stimuli making them extremely good sensors. For example, using the center-of-mass motions of such particles zeptonewton scale force sensitivity has been achieved [17]. Likewise, exploiting the rotational motion of a levitated particle, torque as small as 4.7×0^{-28} N m has been measured [18]. Among levitated particles, magnetic particles are unique in the sense that they contain an extra degree of freedom e.g., the spin which makes them even more versatile. The coupling between the spin and the other degrees of freedom of a levitated magnetic particle has not been explored yet but is promising for developing new technologies and exploring fundamental physics [19]. Recently, levitated magnets in cryogenic conditions have been used for detecting dc magnetic fields [20, 21].

In this article, using the precessional motion of a levitated magnetic particle in ultra-high vacuum, it is shown that extremely weak electromagnetic waves of strength femtotesla (3×10^{-7} V/m) can be detected. Such a magnetometer has a dynamic range over a millitesla, can be continuously tuned for many GHz and detect frequencies with sub-hertz precessions. It is also shown that the direction of arrival of the EM wave can be determined relatively easily.

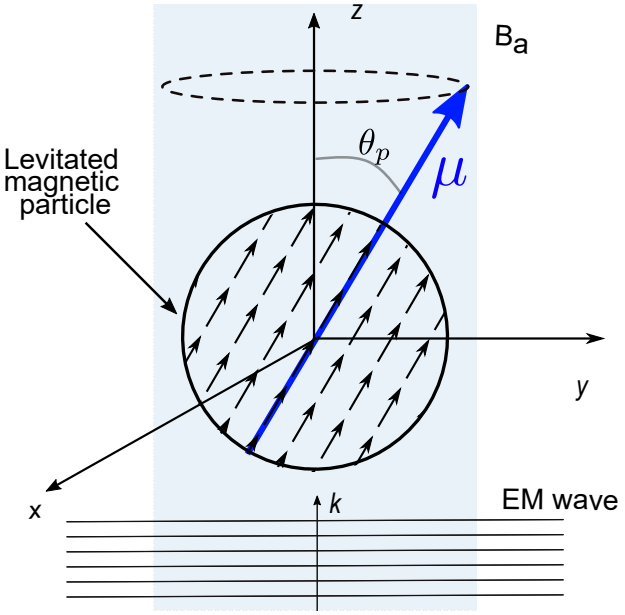

FIG. 1. Precession of a levitated magnet when exposed to electromagnetic waves. The light blue background represents a homogeneous dc magnetic field B_a. A circularly polarized electromagnetic (EM) wave propagating along the z axis initiates spin precession which subsequently induces a mechanical precession. The mechanical angle of precession is denoted by θ_p. The wavevector of the electromagnetic wave is represented by $\mathbf{k}$. The magnetic field associated with the EM wave is in the $x - y$ plane.

Consider a magnetic sphere of moment $\boldsymbol{\mu}$ polarized along its easy magnetization axis is levitated inside a vacuum chamber. A homogeneous dc magnetic field B_a is applied along the $+z$ axis which ensures $\boldsymbol{\mu}$ aligns with B_0 (Fig. 1) i.e., $\boldsymbol{\mu} = [0\ 0\ \mu_s]$, where μ_s is the saturated magnetic moment of the levitated particle. Consider also that an electromagnetic plane wave whose frequency (ω)

and strength we aim to determine is propagating in the $+z$ direction and illuminates the magnetic particle. The interaction between the EM wave and the spins or magnetization initiates a spin precession in the ferromagnetic particle [22, 23] giving rise to components of magnetic moment in the xy plane. The dynamics of spin precession can be modeled using the Landau-Lifshitz-Gilbert equation [23]

$$\frac{d\boldsymbol{\mu}}{dt} \;=\; \gamma\boldsymbol{\mu}\times\mathbf{B} - \frac{\alpha}{\mu_s}(\boldsymbol{\mu}\times\frac{d\boldsymbol{\mu}}{dt}), \qquad (1)$$

where $\mathbf{B} = b_0\cos\omega t\ \hat{x} + \sigma b_0\sin\omega t\ \hat{y} + B_0\ \hat{z}$, γ is the gyromagnetic ratio, $B_0 = B_a + B_{an}$ with B_{an} being the effective field associated with the magnetocrystalline anisotropy, and $\alpha > 0$ is the dimensionless Gilbert damping constant. $\mathbf{b} = b_0\cos\omega t\ \hat{x}+\sigma b_0\sin\omega t\ \hat{y}$ is the magnetic component of the EM field and σ determines its direction of rotation e.g., $\sigma = -1$ $(+1)$ corresponds to clockwise (anticlockwise) rotation. $\mathbf{b}$ is the field that we aim to detect. Equation (1) has no general analytical solution. However, when $b \ll B_0$, one can approximate $\mu_z \approx \mu_s$ and $\frac{d\mu_z}{dt} \approx 0$. Under these conditions [24, 25], the steady state solution of (1) is given by

$$\mu_x \;=\; \frac{b_0\gamma m_s}{\sqrt{(\gamma B_0+\sigma\omega)^2+\alpha^2\omega^2}}\cos(\omega t-\beta), \qquad (2)$$

where β is the phase difference between $\mathbf{b}$ and the precession of spins or magnetization and is given by $\beta = \tan^{-1}[\frac{\alpha\omega}{\gamma B_0+\sigma\omega}]$. A similar expression for μ_y exists and can be found in the supplementary material. Importantly, when $\sigma = -1$, μ_x has a Lorentzian profile and has a full-width half-maximum linewidth of $\approx \sqrt{12\alpha^2\gamma^2B_0^2}$. μ_x reaches its maximum when $\omega = \gamma B_0$. This is known as the ferromagnetic resonance (FMR). On FMR the amplitude of μ_x is $b_x\mu_s/\alpha B_0$. In contrast, when $\sigma = +1$, the rotating EM field opposes the precession of the magnetization [26] and hence the induced magnetic moment in the $x-y$ plane is several orders of magnitude smaller compared to the FMR case since, in our case, ω is in gigahertz and for most material [27–30] $0 < \alpha \ll 1$. Note that when $\mathbf{B_a}$ is applied along the $-z$ axis, a counterclockwise rotating ($\sigma = +1$) EM field can excite FMR [26].

In a ferromagnetic material spins and thus magnetization are connected to the crystal lattice via magnetocrystalline anisotropy [22]. This provides a link between the internal (spin) and the mechanical degrees of freedom of a magnetic object. For a levitated magnet, this connectivity means that when the magnetization starts to precess, the lattice and thus the levitated particle attempt to follow it [21, 24, 31, 32]. Precessions of levitated magnets can be detected using the optical interferometric scheme used in levitated optomechanics [18, 33–35]. For a levitated magnet to precess mechanically, however, it must overcome the resistance that it encounters from the residual gas molecules inside the vacuum chamber. The resistive torque [36] that an object faces at a precession frequency Ω_p is $I\Omega_p\Gamma_g$, where I is the moment of inertia, and Γ_g is the damping rate due to gas molecules. In contrast, the driving torque due to the incoming EM field is given by the right hand side of (1) normalized by γ [22]. At equilibrium when the driving and the resistive torques are equal, the precession frequency is

$$\Omega_p \;=\; \frac{1}{I\Gamma_g}\frac{b_0\mu_s\omega}{\sqrt{(\gamma B_0+\sigma\omega)^2+\alpha^2\omega^2}}, \qquad (3)$$

Equation (3) alone cannot uniquely determine the frequency of the unknown EM wave. This is because when the driving torque is less than the resistive torque, the magnet would precess at a lower rate and hence taking the mechanical precession rate as the frequency of the EM wave would be inaccurate. This, however, can be avoided by measuring the precession frequency as a function of the damping rate or the gas pressure P ($\Gamma_g \propto P$). As P decreases, Ω_p increases. But, when Ω_p reaches the frequency of the unknown EM field, Ω_p remains constant as Γ_g decreases. This is a consequence of the driven nature of mechanical motions which prefer to synchronize with the frequency of the driving fields [24, 31] (see (2)). At the critical damping rate Γ_g^c where $\Omega_p = \omega$, the mechanical precession frequency directly determines the frequency of the EM wave while the strength of the unknown EM field is

$$b_0 \;=\; \frac{I\Gamma_g^c}{\mu_s}\sqrt{(\gamma B_0+\sigma\omega)^2+\alpha^2\omega^2}. \qquad (4)$$

From (4) it is clear that our detector is most sensitive at the ferromagnetic resonance. The occurrence of FMR can be ensured by checking that the mechanical precession frequency (can be separately measured) is equal to γB_0. Otherwise, B_a can be adjusted such that it matches the mechanical precession frequency. Moreover, since on FMR the driving torque is maximum, the mechanical precession at γB_0 is expected to happen at a higher Γ_g^c compared to non-resonant cases. When the FMR condition is satisfied, the minimum detectable field is

$$b_0 \;=\; \frac{2\alpha\rho\gamma B_0\Gamma_g^c r^2}{5M}, \qquad (5)$$

where we have substituted $I = 2\rho v r^2/5$ and $\mu_s = vM$ with r, ρ, v and M being the radius, the mass density, the volume and the saturation magnetization of the levitated magnet. Parameters such as ρ and M in (5) can be found from the relevant bulk material while α, Γ_g^c and r can be measured experimentally in situ [28, 37, 38].

Let us consider numerical examples. Any magnetic materials can be used as long as they can be levitated.

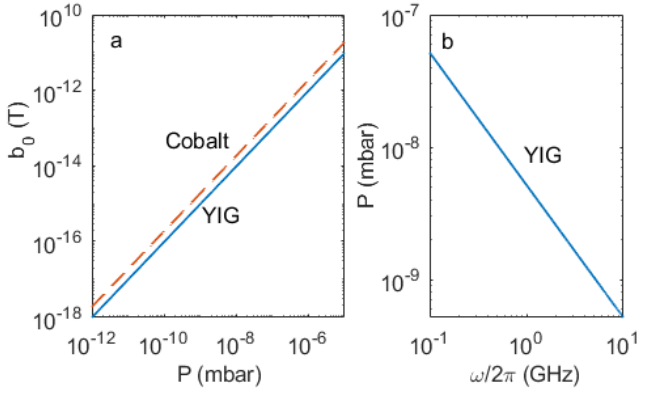

FIG. 2. a) The minimum detectable magnetic field as a function of residual gas pressure when the precession frequency or the frequency of the unknown EM wave is 5 GHz with a YIG ($M = 1.4 \times 10^5$ A/m and $\alpha = 5.58 \times 10^{-5}$) or a cobalt ($M = 1.4 \times 10^6$ A/m and $\alpha = 0.01$) sphere ($r = 100$ nm) as a sensor. b) The minimum required gas pressure for sensing EM fields of different frequencies with $b_0 = 10^{-15}$ T when a YIG sphere (100 nm) is used.

Levitation can be carried out either using a Paul trap [39–41] or optical tweezers [17, 18, 38, 42, 43]. Figure 2a shows the minimum detectable field as a function of the residual gas pressure when a yttrium iron garnet (YIG, a weak magnet) or a cobalt (a strong magnet) sphere ($r = 100$ nm) is used as a sensor. The frequency of the EM field is assumed to be $\omega/2\pi = 5$ GHz and is resonant with the FMR of the levitated magnet. We also used $\Gamma_g \approx \frac{4P}{\rho r v_g}$ with v_g being the velocity of gas molecules [44]. At an experimentally viable pressure of $P = 10^{-9}$ mbar ($\Gamma_g = 2.41 \times 10^{-6}$ rad.), the minimum detectable field is $\approx 2 \times 10^{-15}$ T with cobalt and $\approx 1 \times 10^{-15}$ T with YIG. When converted to electric fields (cb_0), these are equivalent to 6×10^7 V/m and 3×10^7 V/m, respectively, where c is the speed of light. It is evident that despite cobalt being a strong magnet, YIG is preferable. This is because YIG has a significantly lower Gilbert damping constant [27, 28] compared to cobalt [29] resulting in a lower α/M ratio which provides better sensitivities. At a higher vacuum, which is within experimental reach, even better sensitivities seem feasible (Fig. 2a). Assuming that the target sensitivity is 10^{-15} T, Fig. 2b shows the minimum required residual gas pressure as a function of ω when a YIG sphere is used as a sensor. Evidently, EM fields of lower frequencies can be detected at higher gas damping. This is because, at a lower precession frequency, the resistive torque is lower ($\propto \Omega_p$). It is also evident that smaller levitated magnets are better sensors since such objects have significantly lower moments of inertia ($\propto r^5$) requiring smaller driving torques for initiating precessions.

An essential attribute of an EM sensor is to detect signals of different frequencies. Here, this can be accomplished in a resonant manner by adjusting B_a, see (2). As B_a changes, the frequency of the ferromagnetic resonance changes along with it. B_a can be delivered using an electromagnet allowing the detection of arbitrary frequencies within the range of operation of our magnetometer. The highest frequency that our sensor can detect is limited by the maximum tensile stress ($\approx \rho\Omega_p^2 r_p^2$), arising from the mechanical precession, that a levitated magnet can withstand [45, 46], where r_p depends on θ. Mechanical rotations over 5 GHz have been demonstrated [18] and tens of GHz have been predicted [46]. The lowest frequency that a precessing magnetometer can sense is determined by the saturation magnetization and/or the magnetocrystalline anisotropy of a levitated magnet. In this context, weak magnets such as YIG are preferable since their saturation magnetizations are low. Using levitated YIG spheres as sensors, frequencies in the MHz range can be detected [47, 48].

Magnetometers capable of detecting frequencies within a narrow band are highly sought after in spectroscopy [9]. At a given B_a, our magnetometer is sensitive to frequencies within the ferromagnetic resonance linewidth which is dictated by the Gilber damping constant e.g., $\approx \sqrt{12\alpha^2\gamma^2 B_0^2}$. For a high selectivity, materials with low α's are essential. In this regard, YIG is an excellent candidate which is known for its extremely narrow FMR linewidth [27, 28, 49]. Using YIG spheres as sensors frequency selectivity of a few MHz can be achieved [9]. Importantly, within this frequency band, our magnetometer can resolve frequencies with a sub-hertz resolution. This is a result of highly accurate frequency measurements of driven oscillators. For example, rotation frequencies of driven levitated objects have been measured with accuracies better than a mHz [50, 51].

The ability to detect fields of different strengths is known as the dynamic range of a sensor. In our case, it is determined by the angle of precession assuming that a levitated magnet is already precessing at ω. As the strength of the EM field increases, a levitated magnet continues to precess at ω. However, its angle of precession (Fig. 1) increases. This remains true as long as the strength of the unknown magnetic field is $\ll B_a$. If the unknown field becomes comparable to B_a, the approximation made in deriving (2) e.g., $b_0 \ll B_a$ breaks down. Interestingly, as the precession angle increases with the increasing b_0, the detection of precession becomes easier implying an enhanced sensitivity. This is in contrast with other magnetometers which become less sensitive as the strength of the field increases [13, 14, 16]. Generally, B_a is in tens of millitesla implying a large dynamic range e.g., femtotesla to millitesla for a levitated magnet-based magnetometer.

The direction of arrival (DA) of an EM wave is important in many areas of engineering and physics including in defense [52, 53] and astrophysics [2]. In our case, the direction of arrival $\mathbf{k}$ can be found from the direc-

tion of $\mathbf{B_a}$. In deriving (4) we assumed that $\mathbf{b}$ is in the $x-y$ plane and hence, in this simple case, the direction of arrival is along the z axis. To further differentiate between the arrival along the $-z$ and the $+z$ directions, the sensor, due to its small size (equivalent to a small vacuum chamber), can be temporarily blocked using an EM absorber [54] from one of the two sides. In the event the EM arrives from the blocked side, the levitated magnet will stop precessing thus determining the arrival direction. For an arbitrary arrival, the direction of $\mathbf{B_a}$ can be adjusted such that $\mathbf{b}$ becomes perpendicular to $\mathbf{B_0}$. This can be ensured by checking that the maximum precession frequency ($\Omega_p = \omega$, see above) is achieved at the highest possible Γ_g^c. This is because when $\mathbf{k}$ is not parallel to $\mathbf{B_a}$, the magnetic component of the EM wave is not orthogonal to $\mathbf{B_a}$. As a result, the torque exerted by $\mathbf{b}$ is not maximal (see Eq. (3)) requiring a reduced Γ_g^c for the magnet to precess at ω. In the extreme case, when $\mathbf{k} \perp \mathbf{B_a}$, there is no torque and the magnet cannot precess.

In conclusion, we have theoretically shown that a levitated magnet in high vacuum is capable of detecting electromagnetic fields with a femtotesla sensitivity. When converted to an electric field, this is better than a 3×10^{-7} V/m. Benefits of the new magnetometer include a large dynamics range covering from femtotesla to millitesla, highly accurate frequency measurements with a resolution better than a mHz, a large frequency range of operation from MHz to tens of GHz, and a high selectivity. With its high sensitivity, the new magnetometer can potentially be used as a radar receiver. Importantly, due to its high sensitivity and the ability to be configured to sense different frequencies by merely changing the externally applied magnetic field, it can be useful in fields including biomedicine [5, 6], search and rescue [7] and defense [7] where the ability to sense at different frequencies is crucial.

* Department of Physics,University of Warwick, Coventry, UK; anishur.rahman@warwick.ac.uk

[1] A. A. Penzias and R. W. Wilson, A Measurement of Excess Antenna Temperature at 4080 Mc/s., Astrophiscal Journal **142**, 419 (1965).

[2] D. Thornton, B. Stappers, M. Bailes, B. Barsdell, S. Bates, N. D. R. Bhat, M. Burgay, S. Burke-Spolaor, D. J. Champion, P. Coster, N. D'Amico, A. Jameson, S. Johnston, M. Keith, M. Kramer, L. Levin, S. Milia, C. Ng, A. Possenti, and W. van Straten, A population of fast radio bursts at cosmological distances, Science **341**, 53 (2013).

[3] A. T. M. A. Rahman, Ultrawideband axion search using a faraday haloscope, Phys. Rev. D **106**, 115017 (2022).

[4] A. Spezio, Electronic warfare systems, IEEE Trans. Microw. Theory Tech. **50**, 633 (2002).

[5] C. Li, V. M. Lubecke, O. Boric-Lubecke, and J. Lin, A review on recent advances in doppler radar sensors for noncontact healthcare monitoring, IEEE Trans. Microw. Theory Tech. **61**, 2046 (2013).

[6] L. Zhao, C. Yao, H. Wang, J. Dong, J. Zhang, X. Xu, H. Wang, B. Yao, K. Ren, L. Sun, and R. Peng, Immune responses to multi-frequencies of 1.5 ghz and 4.3 ghz microwave exposure in rats: Transcriptomic and proteomic analysis, International Journal of Molecular Sciences **23**, 10.3390/ijms23136949 (2022).

[7] N. Thi Phuoc Van, L. Tang, V. Demir, S. F. Hasan, N. Duc Minh, and S. Mukhopadhyay, Review-microwave radar sensing systems for search and rescue purposes, Sensors **19**, 10.3390/s19132879 (2019).

[8] G. F. Pedersen and H. Gao, Mobile phone antenna performance 2023, Institut for Elektroniske Systemer, Aalborg Universitet. (2023).

[9] C. T. Fancher, D. R. Scherer, M. C. S. John, and B. L. S. Marlow, Rydberg atom electric field sensors for communications and sensing, IEEE Transactions on Quantum Engineering **2**, 1 (2021).

[10] M. Jing, Y. Hu, J. Ma, H. Zhang, L. Zhang, L. Xiao, and S. Jia, Atomic superheterodyne receiver based on microwave-dressed rydberg spectroscopy, Nat. phys. **16**, 911 (2020).

[11] J. Yuan, W. Yang, M. Jing, H. Zhang, Y. Jiao, W. Li, L. Zhang, L. Xiao, and S. Jia, Quantum sensing of microwave electric fields based on rydberg atoms, Reports on Progress in Physics **86**, 106001 (2023).

[12] J. A. Gordon, M. T. Simons, A. H. Haddab, and C. L. Holloway, Weak electric-field detection with sub-1 Hz resolution at radio frequencies using a Rydberg atom-based mixer, AIP Advances **9**, 045030 (2019), https://pubs.aip.org/aip/adv/article-pdf/doi/10.1063/1.5095633/12853333/045030_1_online.pdf.

[13] D. Budker and M. Romalis, Optical magnetometry, Nature physics **3**, 227 (2007).

[14] S. Graham, A. Rahman, L. Munn, R. Patel, A. Newman, C. Stephen, G. Colston, A. Nikitin, A. Edmonds, D. Twitchen, M. Markham, and G. Morley, Fiber-coupled diamond magnetometry with an unshielded sensitivity of $30\,\mathrm{pT}/\sqrt{\mathrm{hz}}$, Phys. Rev. Appl. **19**, 044042 (2023).

[15] J. Meinel, V. Vorobyov, B. Yavkin, D. Dasari, H. Sumiya, S. Onoda, J. Isoya, and J. Wrachtrup, Heterodyne sensing of microwaves with a quantum sensor, Nature communications **12**, 2737 (2021).

[16] F. Couëdo, E. Recoba Pawlowski, J. Kermorvant, J. Trastoy, D. Crété, Y. Lemaître, B. Marcilhac, C. Ulysse, C. Feuillet-Palma, N. Bergeal, and J. Lesueur, High-Tc superconducting detector for highly-sensitive microwave magnetometry, Applied Physics Letters **114**, 192602 (2019).

[17] G. Ranjit, M. Cunningham, K. Casey, and A. A. Geraci, Zeptonewton force sensing with nanospheres in an optical lattice, Phys. Rev. A **93**, 053801 (2016).

[18] J. Ahn, Z. Xu, J. Bang, P. Ju, X. Gao, and T. Li, Ultrasensitive torque detection with an optically levitated nanorotor, Nature nanotechnology **15**, 89 (2020).

[19] A. T. M. A. Rahman, Large spatial schrödinger cat state using a levitated ferrimagnetic nanoparticle, New J. Phys. **21**, 113011 (2019).

[20] F. Ahrens, W. Ji, D. Budker, C. Timberlake, H. Ulbricht, and A. Vinante, Levitated ferromagnetic magnetometer with energy resolution well below $\hbar$ (2024),

arXiv:2401.03774 [quant-ph].
[21] D. F. Jackson Kimball, A. O. Sushkov, and D. Budker, Precessing ferromagnetic needle magnetometer, Phys. Rev. Lett. **116**, 190801 (2016).
[22] C. Kittel, *Introduction to solid state physics*, 8th ed. (Wiley, Hoboken, N.J, 2005).
[23] T. L. Gilbert, A phenomenological theory of damping in ferromagnetic materials, IEEE Trans. Magn. **40**, 3443 (2004).
[24] H. Xi, K.-Z. Gao, Y. Shi, and S. Xue, Precessional dynamics of single-domain magnetic nanoparticles driven by small ac magnetic fields, Journal of Physics D: Applied Physics **39**, 4746 (2006).
[25] C. Mitsumata and S. Tomita, Control of gilbert damping using magnetic metamaterials, Phys. Rev. B **84**, 174421 (2011).
[26] S. I. Denisov, T. V. Lyutyy, and P. Hänggi, Magnetization of nanoparticle systems in a rotating magnetic field, Phys. Rev. Lett. **97**, 227202 (2006).
[27] H. Chang, P. Li, W. Zhang, T. Liu, A. Hoffmann, L. Deng, and M. Wu, Nanometer-thick yttrium iron garnet films with extremely low damping, IEEE Magn. Lett. **5**, 1 (2014).
[28] H. Maier-Flaig, S. Klingler, C. Dubs, O. Surzhenko, R. Gross, M. Weiler, H. Huebl, and S. T. B. Goennenwein, Temperature-dependent magnetic damping of yttrium iron garnet spheres, Phys. Rev. B **95**, 214423 (2017).
[29] F. Schreiber, J. Pflaum, Z. Frait, T. Mühge, and J. Pelzl, Gilbert damping and g factor in Fe˙xCo1˙x alloy films, Solid State Communications **93**, 965 (1995).
[30] E. Barati and M. Cinal, Gilbert damping in binary magnetic multilayers, Phys. Rev. B **95**, 134440 (2017).
[31] H. Keshtgar, S. Streib, A. Kamra, Y. M. Blanter, and G. E. W. Bauer, Magnetomechanical coupling and ferromagnetic resonance in magnetic nanoparticles, Phys. Rev. B **95**, 134447 (2017).
[32] P. Fadeev, C. Timberlake, T. Wang, A. Vinante, Y. B. Band, D. Budker, A. O. Sushkov, H. Ulbricht, and D. F. J. Kimball, Ferromagnetic gyroscopes for tests of fundamental physics, Quantum Science and Technology **6**, 024006 (2021).
[33] M. Rashid, M. Toroš, A. Setter, and H. Ulbricht, Precession motion in levitated optomechanics, Phys. Rev. Lett. **121**, 253601 (2018).
[34] A. T. M. A. Rahman, A. C. Frangeskou, P. F. Barker, and G. W. Morley, An analytical model for the detection of levitated nanoparticles in optomechanics, Rev. Sci. Instrum. **89**, 023109 (2018).
[35] R. Reimann, M. Doderer, E. Hebestreit, R. Diehl, M. Frimmer, D. Windey, F. Tebbenjohanns, and L. Novotny, Ghz rotation of an optically trapped nanoparticle in vacuum, Phys. Rev. Lett. **121**, 033602 (2018).
[36] S. Kuhn, A. Kosloff, B. A. Stickler, F. Patolsky, K. Hornberger, M. Arndt, and J. Millen, Full rotational control of levitated silicon nanorods, Optica **4**, 356 (2017).
[37] A. T. M. A. Rahman, A. C. Frangeskou, M. S. Kim, S. Bose, G. W. Morley, and P. F. Barker, Burning and graphitization of optically levitated nanodiamonds in vacuum, Sci. Rep. **6** (2016).
[38] A. T. M. A. Rahman and P. F. Barker, Measurement of the motional heating of a levitated nanoparticle by thermal light, Phys. Rev. A **107**, 013521 (2023).
[39] T. W. Penny, A. Pontin, and P. F. Barker, Sympathetic cooling and squeezing of two colevitated nanoparticles, Phys. Rev. Res. **5**, 013070 (2023).
[40] T. Delord, L. Nicolas, L. Schwab, and G. Hétet, Electron spin resonance from NV centers in diamonds levitating in an ion trap, N. J. Phys. **19**, 033031 (2017).
[41] D. S. Bykov, L. Dania, F. Goschin, and T. E. Northup, 3d sympathetic cooling and detection of levitated nanoparticles, Optica **10**, 438 (2023).
[42] J. Vovrosh, M. Rashid, D. Hempston, J. Bateman, M. Paternostro, and H. Ulbricht, Parametric feedback cooling of levitated optomechanics in a parabolic mirror trap, J. Opt. Soc. Am. B **34**, 1421 (2017).
[43] A. T. M. A. Rahman and P. F. Barker, Optical levitation using broadband light, Optica **7**, 906 (2020).
[44] S. A. Beresnev, V. G. Chernyak, and G. A. Fomyagin, Motion of a spherical particle in a rarefied gas. part 2. drag and thermal polarization, J. Fluid Mech. **219**, 405–421 (1990).
[45] M. Schuck, D. Steinert, T. Nussbaumer, and J. W. Kolar, Ultrafast rotation of magnetically levitated macroscopic steel spheres, Sci. adv. **4** (2018).
[46] J. Ahn, Z. Xu, J. Bang, Y.-H. Deng, T. M. Hoang, Q. Han, R.-M. Ma, and T. Li, Optically levitated nanodumbbell torsion balance and ghz nanomechanical rotor, Phys. Rev. Lett. **121**, 033603 (2018).
[47] S. Lee, S. Grudichak, J. Sklenar, C. C. Tsai, M. Jang, Q. Yang, H. Zhang, and J. B. Ketterson, Ferromagnetic resonance of a YIG film in the low frequency regime, J. Appl. Phys. **120**, 033905 (2016), https://pubs.aip.org/aip/jap/article-pdf/doi/10.1063/1.4956435/13239633/033905_1_online.pdf.
[48] P. H. Bryant, T. L. Carroll, L. M. Pecora, and F. J. Rachford, Subsaturation ferromagnetic resonance in yttrium iron garnet spheres, Appl. Phys. Lett. **61**, 864 (1992), https://pubs.aip.org/aip/apl/article-pdf/61/7/864/18490713/864_1_online.pdf.
[49] A. A. Serga, A. V. Chumak, and B. Hillebrands, YIG magnonics, J. Phys. D **43**, 264002 (2010).
[50] Y. Jin, K. Shen, P. Ju, X. Gao, C. Zu, A. J. Grine, and T. Li, Quantum control and fast rotation of levitated diamonds in high vacuum (2023).
[51] S. Kuhn, B. A. Stickler, A. Kosloff, F. Patolsky, K. Hornberger, M. Arndt, and J. Millen, Optically driven ultrastable nanomechanical rotor, Nat. Commun. **8**, 1 (2017).
[52] A. K. Robinson, N. Prajapati, D. Senic, M. T. Simons, and C. L. Holloway, Determining the angle-of-arrival of a radio-frequency source with a Rydberg atom-based sensor, Appl. Phys. Lett. **118**, 114001 (2021).
[53] M. Huang, B. Zheng, T. Cai, X. Li, J. Liu, C. Qian, and H. Chen, Machine–learning-enabled metasurface for direction of arrival estimation, Nanophotonics **11**, 2001 (2022).
[54] M. F. Elmahaishi, R. S. Azis, I. Ismail, and F. D. Muhammad, A review on electromagnetic microwave absorption properties: their materials and performance, J MATER RES TECHNOL **20**, 2188 (2022).